ISSN 1814-4225 (print)
ISSN 2663-2012 (online)

UDC 621.3:004.932 **doi: 10.32620/reks.2025.4.14**

Maksym RYBNYTSKYI, Sergii KRYVENKO, Volodymyr LUKIN, Volodymyr REBROV

National Aerospace University "Kharkiv Aviation Institute", Kharkiv, Ukraine

A COMBINED APPROACH TO PIXEL-WISE CLASSIFICATION OF SATELLITE IMAGES BASED ON LBP, PSEUDOCOLOR FEATURES, AND XGBOOST

The subject *of the article is pixel-wise classification of Sentinel-2 satellite imagery represented as three-channel data mapped to the RGB color space for convenient visualization, with specific attention to the challenges posed by sensor noise and lossy compression artifacts typical for satellite data.* ***The goal*** *is to develop and validate a classification approach that maintains high accuracy under substantial noise and compression, by combining Local Binary Patterns (LBP) texture descriptors with pseudocolor features and employing an efficient ensemble classifier.* ***The tasks to be addressed*** *are: to design a compact feature representation that integrates LBP-based texture information with pseudocolor; to train and tune an XGBoost classifier on these features and compare its performance with baselines that rely on pseudocolor information alone and with simple neural network models; to assess robustness to noise and compression artifacts across a range of compression levels.* ***The methods*** *used include extraction of LBP descriptors to capture local texture patterns, construction of pseudocolor features from RGB-mapped Sentinel-2 channels, and concatenation of these descriptors into joint feature vectors. An XGBoost algorithm is employed to build the classification model. Model effectiveness is evaluated using the F1 score as the primary metric under varying noise and compression conditions. Visual inspection of the resulting classification maps is used to corroborate quantitative results and to analyze spatial consistency and error patterns.* ***Conclusions****. The scientific novelty of the results is as follows: for the first time in the context of Sentinel-2 pixel-wise classification, the use of LBP in combination with XGBoost has been systematically investigated and substantiated for BPG lossy compression scenarios at the optimal operating point (OOP) or nearby; it has been experimentally established that there is a substantial gain in classification accuracy for heterogeneous classes (urban areas, vegetation, bare soil) and a limited gain for homogeneous ones (water), and interaction artifacts of BPG+LBP on homogeneous surfaces have been documented, with directions outlined for adapting LBP parameters to mitigate them; the computational suitability of the approach (feature extraction, training, and classification time) for operational pipelines has been demonstrated; a comparison with a simple neural network has been conducted showing higher stability of the proposed approach on texture-rich classes under noise and compression, thereby delineating the limits of applicability of alternative methods. The study also shows that accounting for compression effects is important for operational processing pipelines: compressing images to an optimal operating point can reduce data volume and, in some cases, slightly improve classification accuracy by attenuating noise.*

Keywords: *classification; satellite imagery; Local Binary Patterns; XGBoost; noise; compression.*

1. Introduction

1.1. Motivation

Satellite image classification is one of the key tasks in Earth remote sensing [1, 2]. Satellites such as Sentinel-1 and Sentinel-2 provide vast volumes of high-quality data, including radar and multispectral imagery, which are used across a wide range of application domains. In pixel-wise classification, each pixel of a satellite image must be assigned to a specific class (e.g., water, vegetation, soil, buildings). However, this approach faces several challenges.

Data complexity. Satellite images often exhibit high levels of noise caused by both sensor characteristics and atmospheric phenomena during data acquisition. This noise can cause significant signal distortion [3] and make worse classification accuracy. Moreover, images may display feature-space overlap between different classes, complicating their discrimination. The intrinsic heterogeneity of the Earth's surface also affects the data [4].

Data compression. Given the massive volume of information collected by sensors onboard satellites, compression is widely used to enable efficient transmission and storage. Although lossless compression preserves all image information, in practice lossy compression is used in most cases due to bandwidth and storage constraints [5]. Therefore, it is important that classification algorithms be robust not only to noise but also operate effectively on compressed data, whose distortions often resemble noise [6], while maintaining high classification accuracy.

Limited use of context. Pixel-wise approaches

largely focus only on the characteristics of individual pixels and ignore spatial relationships among neighboring pixels. However, these relationships can carry important information that can substantially improve classification effectiveness and accuracy [7, 8].

1.2. State of the art

Satellite-derived data are vital for tasks like drought monitoring, land management, urban planning, and climate modeling [4, 9]. Modern remote sensing datasets provide accurate surface characteristics, essential for Earth analysis and classification [10].

Classification of satellite data is critical in many practical applications [11]. Satellites such as Sentinel-1 and Sentinel-2 generate massive volumes of data at relatively high spatial resolution. Compressing such data is a common and essential step because it can greatly reduce volume with no loss or only minimal loss of useful information. Modern compression algorithms [5] are designed to combine high compression ratios with the preservation of features important for downstream analysis. In the context of remote sensing, data compression is crucial for efficient transmission from satellites to ground stations and for optimizing computational resources for processing [12].

The impact of lossy compression on satellite image classification has been widely discussed in recent literature. For instance, studies have evaluated the High Efficiency Video Coding (HEVC) intra-frame compression – which serves as the core of the BPG codec – showing its superior performance over JPEG 2000 in crop classification tasks even at high compression ratios [13]. Additionally, the performance of the XGBoost algorithm has been analyzed in the context of compressed remote sensing imagery [14]. Another critical factor is the presence of noise, which significantly affects classification accuracy. Recent studies have explored the impact of different noise types and levels on machine learning techniques [15] and evaluated noise effects on deep learning models in real-time processing scenarios [16].

Furthermore, the combined effect of noise and lossy compression presents a complex challenge. Previous research investigated this interaction using quite old DCT-based coders [17], as well as more recent studies applying the BPG coder to noisy images with pixel-wise neural network classification [18]. However, these works often focus on either spectral features alone or standard neural architectures.

Compression can both reduce noise levels and introduce artifacts that complicate classification. The presence of noise is one of the main challenges in working with satellite data, arising from sensor characteristics as well as acquisition modes and conditions. A particularly important task is selecting compression parameters such that the trade-off between compression and image quality minimizes the impact of artifacts [12]. This trade-off point is referred to as the optimal operating point (OOP). When such a point exists for an image, it enables a compromise between minimizing distortions and preserving key data features required for classification.

Neural networks are often used for the classification of satellite data [19], offering high accuracy and the ability to model complex nonlinear relationships. However, classical algorithms, such as decision tree methods, remain a relevant choice due to their efficiency, ease of implementation, and lower computational demands [20]. We adopt the XGBoost algorithm in this research, known for its high performance and robustness to overfitting [21]. XGBoost requires data preprocessing and the extraction of relevant features for effective operation. In general, both spectral and spatial features can be used for classification. A pixel's spectral representation is a vector of values comprising all or selected channels, while the spatial representation includes information about neighboring pixels and their relationships [22]. In the context of pixel-wise classification of satellite data, the use of Local Binary Patterns (LBP) is a particularly suitable choice [23].

LBP is a simple yet effective texture operator. Its principle is based on comparing the intensities of neighboring pixels around a central pixel against a threshold and encoding the result as a binary value [24]. The logical representation of the basic LBP is shown in Fig. 1.

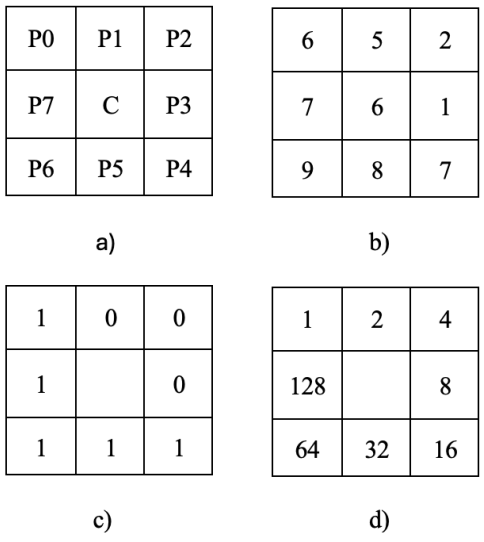

Fig. 1. Original LBP approach: a) binarization template; b) example image patch; c) computed comparison outcomes relative to the central pixel; d) weights (i.e., powers of two)

In the example shown, pixels with values greater than or equal to the central pixel are marked as 1, and those with smaller values as 0. Using the reverse template

ISSN 1814-4225 (print)
ISSN 2663-2012 (online)

order P7 P6 P5 P4 P3 P2 P1 P0, we construct the LBP binary code 11110001. We then convert this binary value to decimal: 128 + 64 + 32 + 16 + 1 = 241. The resulting value serves as an additional LBP feature for the central pixel. While the studies cover 'pair-wise' interactions between noise, compression, and classification, the simultaneous impact of all three components remains insufficiently explored. Despite the popularity of LBP and XGBoost, their combined application has not been systematically studied for satellite imagery processed with modern BPG (Better Portable Graphics) compression under noise conditions. BPG uses different coding logic compared to JPEG or JPEG2000, and its interaction with texture descriptors like LBP remains unexplored, especially at the Optimal Operating Point (OOP). Our research fills this gap by investigating how BPG-induced artifacts and noise affect the stability of LBP features and the subsequent classification performance of XGBoost.

1.3. Objectives and tasks

The goal of this work is to improve pixel-wise classification performance on compressed satellite images affected by noise at the optimal operating point (OOP). Unlike existing studies that focus on standard compression formats, this research explores the synergy between Local Binary Patterns (LBP) [24] and the XGBoost algorithm [25] under BPG-specific distortions.

To achieve this goal, the following tasks were addressed:

1) investigate the impact of controlled noise and BPG (Better Portable Graphics) compression on satellite imagery [26], with a specific focus on identifying the optimal operating point (OOP) where noise reduction and edge/detail preservation are balanced;

2) measure the real benefit of using LBP features under different noise and BPG compression levels to see how much they improve classification compared to using only color data;

3) test the robustness of the combined LBP+XGBoost approach in different cases of data degradation to find the performance limits for both homogeneous and heterogeneous land-cover classes;

4) check the computational efficiency of the method, including the time for feature extraction, model training, and classification, to make sure it is fast enough for practical use.

2. Materials and methods of research

For this study, we selected two Sentinel-2 satellite images previously used in [27] as examples of areas with different levels of structural complexity. Each image has a resolution of 512×512 pixels. These images (see Fig. 2) correspond to regions of the Kharkiv area – a rural locality and an urbanized zone with complex structure.

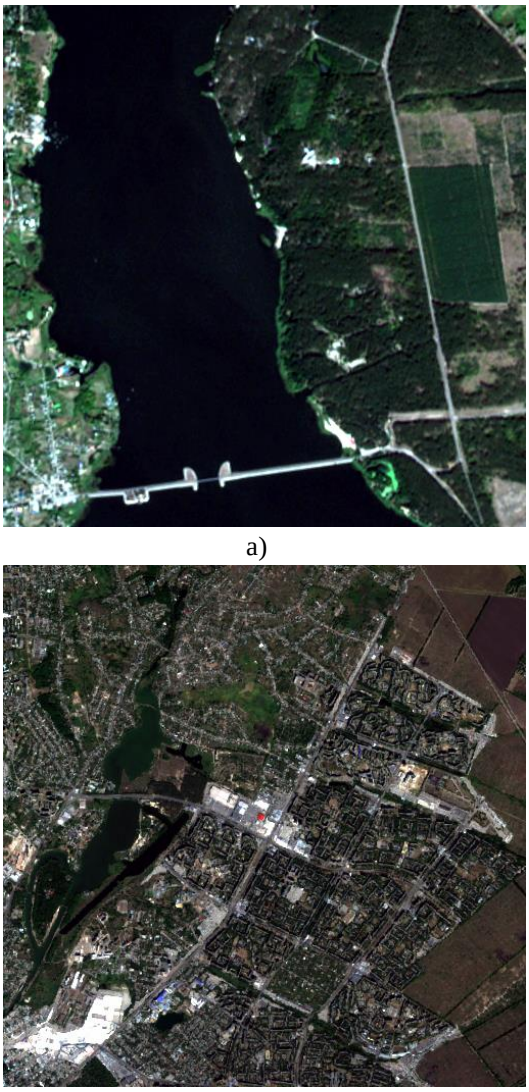

a)

b)

Fig. 2. Test images SS1 (a) and SS2 (b)

Reusing the same scenes is a logical choice, as prior analysis has confirmed their suitability for land-cover classification, specifically for identifying the classes Urban, Water, Vegetation and Bare soil. Thus, the image selection is grounded in previous research, providing a reliable basis for this work.

We adopt the Better Portable Graphics (BPG) encoder as the compression algorithm. BPG is based on intra-coding tools from the HEVC (H.265) video compression standard. At the same file size, images in BPG format typically provide higher quality than other formats [26]. The compression level is controlled by the quality factor Q. Prior studies have shown that, for the same disk capacity, BPG enables storing a larger number of images at the required quality level compared with JPEG and JPEG 2000.

We propose combining local texture descriptors (Local Binary Patterns, LBP) with color information (in this case, three optical bands from the multispectral image mapped to the RGB space) to construct feature vectors. The resulting feature vectors are used to train the XGBoost classifier [25], which is based on decision-tree models. The proposed classification algorithm consists of the following steps:

1) Data Preprocessing: Input image bands are prepared and normalized;

2) Feature Extraction: For each pixel, two types of data are collected: spectral values (RGB) and the local texture code calculated using the LBP operator;

3) Feature Fusion: The RGB values and LBP codes are combined into a single feature vector for every pixel;

4) Model Training/Inference: These combined vectors, along with the corresponding ground-truth masks, are fed into the XGBoost model. During this stage, the algorithm builds a series of decision trees that create logical connections between the pixel features and their respective classes.

This approach targets pixel-wise classification by efficiently extracting informative image features and processing them in a robust learning pipeline.

In practice, the following types of data may be available for training the classifier: 1) images without lossy compression (or lossless compressed); 2) images compressed with losses such that the compression characteristics are close to those of the data to be classified; 3) images compressed with losses whose compression characteristics fully match the target data.

Accordingly, we introduce the following notation: let I_t denote the clean image, I_n the noisy image, $I_c(Q)$ the image compressed with quality parameter Q, I_{QOOP} the image compressed with Q_{OOP}, and I_{QOOP-4} the image compressed with $Q = Q_{OOP}-4$.

To determine the OOP, we use the formula proposed in [12], which is valid for component-wise (per-channel) compression:

$$Q_{OOP} = 14.9 + 20\log_{10}(\sigma), \qquad (1)$$

where σ^2 denotes the noise variance in the image.

In this work, we consider three noise variance levels for Additive White Gaussian Noise (AWGN) – $\sigma^2 = 25$, 50, and 100 – assuming three-channel RGB images with noise independent across channels. These variance levels are used to evaluate the classifier's performance under noisy conditions (see Fig. 3). Let us visualize the possible existence of an optimal operating point. For example, for the highest noise level $\sigma^2 = 100$, according to (1) the predicted Q_{OOP} is Q = 35. Consider the corresponding PSNR curves for both images (Fig. 4), where the peak signal-to-noise ratio $PSNR_{tc}$ is calculated between I_t and the compressed image.

From the plots in Fig. 4(a), it follows that the theoretically obtained OOP value agrees with practical results for PSNR computed between I_t and $I_c(Q)$. However, the example in Fig. 4(b) shows that an OOP may not be observed. In such case, it may be reasonable to compress

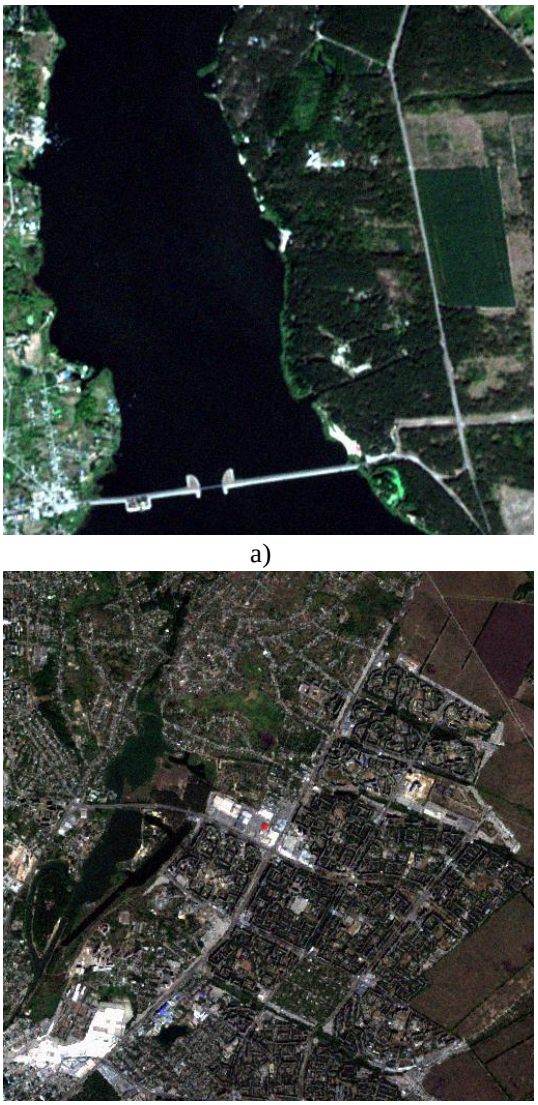

a) b)

Fig. 3. Test images SS1 (a) and SS2 (b) with Additive White Gaussian Noise (AWGN) at $\sigma^2 = 100$

the image at a value different from the Q_{OOP} estimated by (1), but at a slightly lower value, e.g., $Q = Q_{OOP} - 4$. This situation is typical for images of high complexity with many fine details and textures.

The images used (the original SS1 and SS2) are assumed to be nearly noise-free or to have very low noise levels (i.e., they are treated as I_t). Artificial noise with specified characteristics is then added, and the resulting images are compressed using the Q values specified above.

All computations were carried out on a machine configured with an Apple M1 Pro CPU and 32 GB of

ISSN 1814-4225 (print)
ISSN 2663-2012 (online)

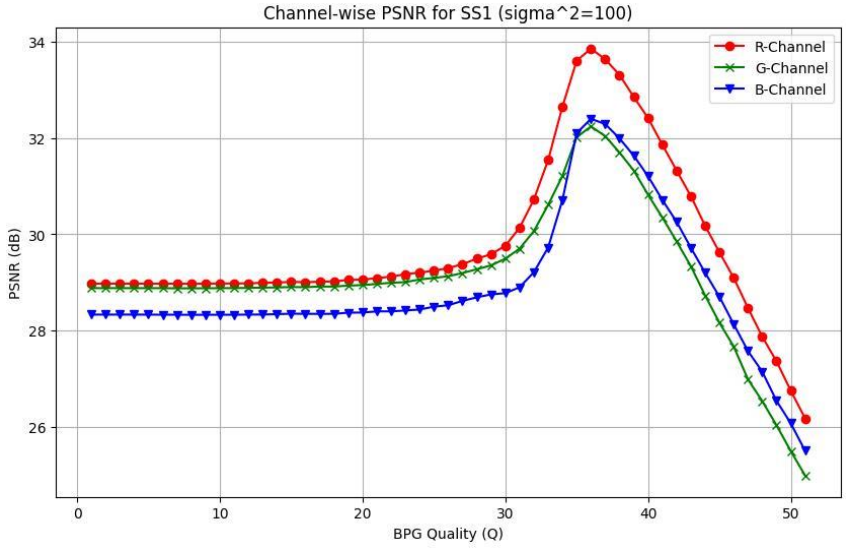

a)

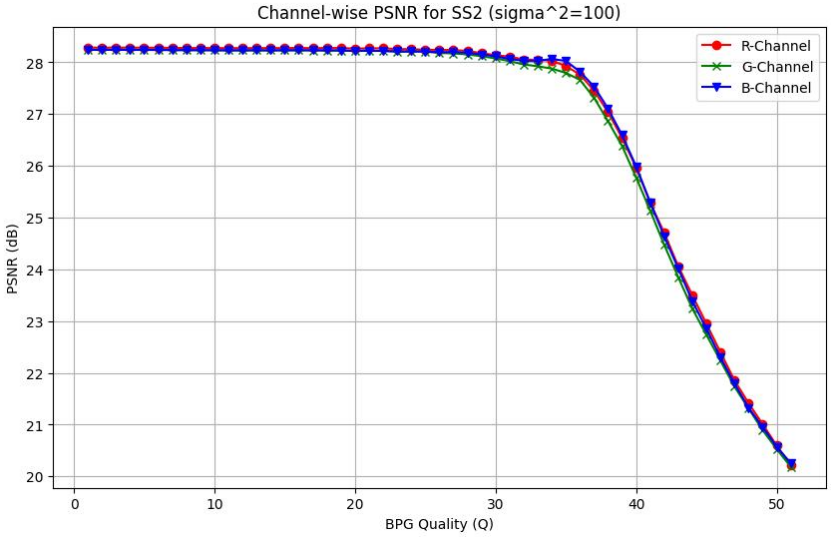

b)

Fig. 4. PSNR(Q) curves for component-wise (per-channel) compression of images SS1 - Image 1 (a) and SS2 – Image 2 (b) using the BPG encoder, $\sigma^2 = 100$

LPDDR5 RAM, using Python. LBP features were computed separately for each channel. By default, the Python XGBoost package provides the following settings: number of trees = 100; maximum depth = 6; learning rate = 0.3. For LBP, the baseline configuration uses a radius of 1 and 8 neighbors [24, 28]. Other configurations are also recommended depending on image complexity [29]. To select optimal classifier hyperparameters, we employed a grid-search procedure [20].

The following hyperparameter grid was proposed for the search:

number of trees (XGBoost): [100, 200, 300, 500];
maximum depth (XGBoost): [4, 6, 8];
learning rate (XGBoost): [0.05, 0.1, 0.3];
radius (LBP): [1, 2, 3];
number of neighbors (LBP): [8, 16, 24].

The optimal parameters were selected based on the best model performance across both images and visual inspection of the classified masks, while also accounting for the time required for training and classification. For this research, the following parameters were chosen:

the number of trees (XGBoost): 500; maximum tree depth (XGBoost): 4; learning rate (XGBoost): 0.3; radius (LBP): 1; number of neighbors (LBP): 8.

3. Results and Discussion

The classifier was trained using three image variants: $I_{n,}$ I_{QOOP} and I_{QOOP-4} – at multiple noise levels, yielding nine models in total, which were then evaluated on each image at the corresponding noise level. The training and validation masks shown in Fig. 5 were used.

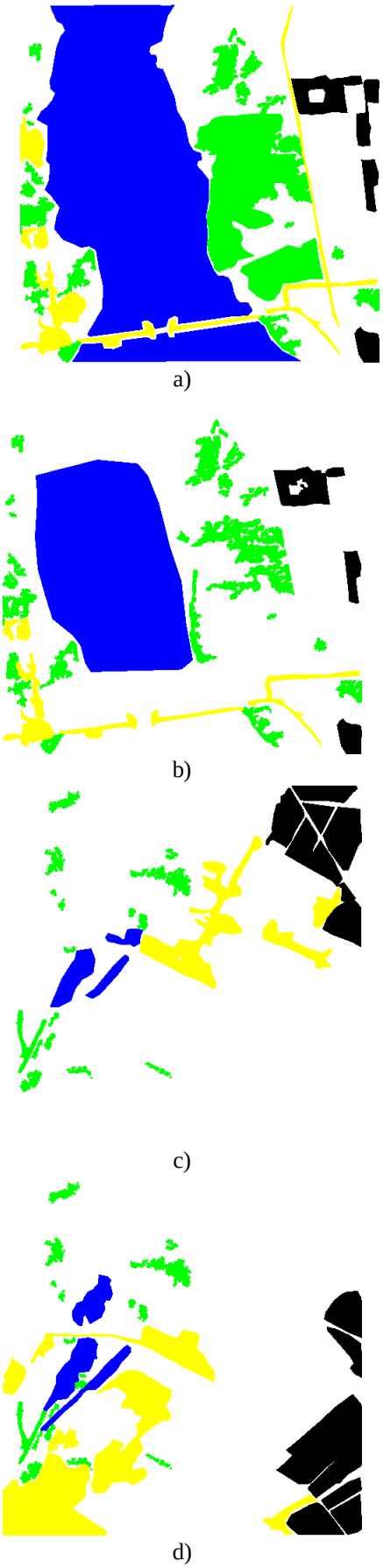

Fig. 5. Fragments used for training (a, c) and validation (b, d) of the model for images SS1 (a, b) and SS2 (c, d)

The masks contain overlapping regions; in the validation mask for SS1, there are 69 451 pixels that do not appear in the training mask and 85 711 that are shared. For SS2, there are 45 243 non-overlapping pixels and 15 071 shared.

All pixels within the respective masks were used for training and validation without additional sampling. Table 1 reports the number of labeled pixels and their distribution across classes for each mask, as well as the number of pixels not used for training.

The F1-score metric was used to assess model accuracy [30].

The contribution of LBP features compared with using only per-channel image information is presented in Table 2 for SS1 and Table 3 for SS2. Let us also explain what is meant by homogeneous and heterogeneous classes. For both images, Water is treated as a homogeneous class, whereas Bare soil, Vegetation, and Urban are considered heterogeneous classes. In SS1, Water forms a large homogeneous region; for this class, adding LBP features improved classification accuracy by only 1–2%. This is because LBP effectively captures local spatial patterns (texture), which are almost absent in uniform water surfaces, making standard spectral data sufficient for this class.

In contrast, for the heterogeneous classes, the improvement ranged from 2% to 17%, with the largest gain observed for Bare soil. This significant increase suggests that texture information is crucial for distinguishing between classes with similar spectral signatures but different surface structures. When comparing results for original versus compressed images, the greatest increase in accuracy was observed at $\sigma^2 = 100$. Across all classes, the inclusion of LBP features yielded accuracy improvements. This indicates that LBP features provide a degree of noise-filtering effect, as they focus on local pixel relationships rather than individual noisy pixel values. For SS2, no single class dominates as in SS1. The overall trend indicates that LBP features improve the accuracy of texture-rich classes. Moreover, at $\sigma^2 = 100$, uncompressed images showed a larger accuracy gain than compressed images.

The results for all classification scenarios using I_n, I_{QOOP} та I_{QOOP-4} for training and validation on image SS1 are presented in Table 4. These scenarios allow evaluating the model's sensitivity to mismatches between the training data quality and the real-world input data.

When using I_n for both training and validation, a slight degradation in the weighted F1-score is observed with increasing σ^2: 0.96 at $\sigma^2 = 25$ and 0.95 at $\sigma^2 = 100$. For I_{QOOP-4}, the same trend persists, with the weighted F1-score decreasing as σ^2 increases. For I_{QOOP}, the metric remained essentially stable regardless of σ^2. The stability of the I_{QOOP} results suggests that optimal compression can act as a regularizer, removing high-frequency noise

ISSN 1814-4225 (print)
ISSN 2663-2012 (online)

that typically confuses the classifier at high σ^2 levels.

When training on I_{QOOP-4} and testing on I_{QOOP-4} and I_{QOOP}, the decreasing trend of the F1 metric with increasing σ^2 persisted. However, the weighted F1 score was higher than in the scenario where I_n was used for training. This confirms that training on data that matches the expected degradation (noise and compression) of the test data is more effective than training on 'clean' images.

The results for SS2 are shown in Table 5. When using I_n for both training and validation, the weighted F1-score decreased slightly as σ^2 increased—from 0.88 at σ^2=25 to 0.87 at σ^2=100. The overall lower F1-scores for SS2 compared to SS1 are likely due to the higher complexity and fragmentation of the classes in the second image.

Table 1

Comparison of the masks used for training and validation of the model

	Total	Urban	Water	Vegetation	Bare soil
Training mask SS1 (pixels)	85983	7441	52310	19936	6296
Validation mask SS1 (pixels)	155162	12154	96852	38258	7898
Difference for SS1 (pixels)	69451	4808	44554	18322	1767
Training mask SS2 (pixels)	36744	11469	4201	5993	15081
Validation mask SS2 (pixels)	60314	28040	7117	6032	19125
Difference for SS2 (pixels)	45243	24434	3792	259	16758

Table 2

Comparative table of classification results with and without LBP features for SS1

Case	σ^2	Training Image	Classified Image	F1, Urban	F1, Water	F1, Vegetation	F1, Bare soil
1. RGB only	25	I_n	I_n	0.84	0.98	0.91	0.80
1. RGB+LBP		I_n	I_n	0.89	0.99	0.94	0.87
2. RGB only		I_{QOPT}	I_{QOPT}	0.86	0.99	0.95	0.83
2. RGB+LBP		I_{QOPT}	I_{QOPT}	0.89	0.99	0.96	0.88
3. RGB only	50	I_n	I_n	0.82	0.97	0.88	0.77
3. RGB+LBP		I_n	I_n	0.88	0.99	0.93	0.86
4. RGB only		I_{QOPT}	I_{QOPT}	0.85	0.99	0.95	0.83
4. RGB+LBP		I_{QOPT}	I_{QOPT}	0.89	0.99	0.96	0.87
5. RGB only	100	I_n	I_n	0.80	0.96	0.84	0.73
5. RGB+LBP		I_n	I_n	0.91	0.98	0.93	0.90
6. RGB only		I_{QOPT}	I_{QOPT}	0.84	0.99	0.95	0.80
6. RGB+LBP		I_{QOPT}	I_{QOPT}	0.88	0.99	0.96	0.86

Table 3

Comparative table of classification results with and without LBP features for SS2

Case	σ^2	Training Image	Classified Image	F1, Urban	F1, Water	F1, Vegetation	F1, Bare soil
1. RGB only	25	I_n	I_n	0.90	0.76	0.61	0.85
1. RGB+LBP		I_n	I_n	0.93	0.79	0.70	0.91
2. RGB only		I_{QOPT}	I_{QOPT}	0.91	0.77	0.66	0.88
2. RGB+LBP		I_{QOPT}	I_{QOPT}	0.93	0.77	0.69	0.90
3. RGB only	50	I_n	I_n	0.89	0.77	0.57	0.82
3. RGB+LBP		I_n	I_n	0.92	0.80	0.69	0.89
4. RGB only		I_{QOPT}	I_{QOPT}	0.91	0.79	0.63	0.86
4. RGB+LBP		I_{QOPT}	I_{QOPT}	0.93	0.78	0.68	0.89
5. RGB only	100	I_n	I_n	0.88	0.77	0.53	0.79
5. RGB+LBP		I_n	I_n	0.92	0.81	0.67	0.87
6. RGB only		I_{QOPT}	I_{QOPT}	0.89	0.77	0.58	0.83
6. RGB+LBP		I_{QOPT}	I_{QOPT}	0.92	0.79	0.66	0.87

Table 4

Classification results for image SS1

Case	σ^2	Training Image	Classified Image	F1 class 3 (Urban)	F1 class 0 (Water)	F1 class 1 (Vegetation)	F1 class 2. (Bare soil)	F1 Total
1	25	I_n	I_n	0.89	0.99	0.94	0.87	0.96
2	25	I_n	I_{QOPT-4}	0.84	0.98	0.93	0.80	0.95
3	25	I_n	I_{QOPT}	0.84	0.99	0.94	0.80	0.96
4	25	I_{QOPT-4}	I_n	0.84	0.97	0.89	0.79	0.93
5	25	I_{QOPT-4}	I_{QOPT-4}	0.89	0.99	0.96	0.88	0.97
6	25	I_{QOPT-4}	I_{QOPT}	0.85	0.99	0.95	0.81	0.96
7	25	I_{QOPT}	I_n	0.80	0.97	0.91	0.78	0.94
8	25	I_{QOPT}	I_{QOPT-4}	0.84	0.99	0.95	0.81	0.96
9	25	I_{QOPT}	I_{QOPT}	0.89	0.99	0.96	0.88	0.97
10	50	I_n	I_n	0.88	0.99	0.93	0.86	0.96
11	50	I_n	I_{QOPT-4}	0.84	0.98	0.91	0.80	0.94
12	50	I_n	I_{QOPT}	0.84	0.97	0.90	0.78	0.93
13	50	I_{QOPT-4}	I_n	0.81	0.97	0.89	0.78	0.93
14	50	I_{QOPT-4}	I_{QOPT-4}	0.89	0.99	0.95	0.87	0.97
15	50	I_{QOPT-4}	I_{QOPT}	0.85	0.99	0.95	0.80	0.96
16	50	I_{QOPT}	I_n	0.81	0.95	0.85	0.76	0.90
17	50	I_{QOPT}	I_{QOPT-4}	0.84	0.99	0.93	0.79	0.95
18	50	I_{QOPT}	I_{QOPT}	0.89	0.99	0.96	0.87	0.97
19	100	I_n	I_n	0.88	0.98	0.92	0.86	0.95
20	100	I_n	I_{QOPT-4}	0.83	0.98	0.91	0.78	0.94
21	100	I_n	I_{QOPT}	0.83	0.84	0.71	0.75	0.80
22	100	I_{QOPT-4}	I_n	0.83	0.98	0.91	0.78	0.94
23	100	I_{QOPT-4}	I_{QOPT-4}	0.88	0.98	0.93	0.85	0.96
24	100	I_{QOPT-4}	I_{QOPT}	0.83	0.96	0.87	0.77	0.92
25	100	I_{QOPT}	I_n	0.75	0.93	0.83	0.74	0.88
26	100	I_{QOPT}	I_{QOPT-4}	0.81	0.96	0.87	0.75	0.91
27	100	I_{QOPT}	I_{QOPT}	0.88	0.99	0.96	0.86	0.97

Table 5

Classification results for image SS2

Case	σ^2	Training Image	Classified Image	F1 class 3 (Urban)	F1 class 0 (Water)	F1 class 1 (Vegetation)	F1 class 2 (Bare soil)	F1 Total
1	25	I_n	I_n	0.93	0.79	0.70	0.91	0.88
2	25	I_n	I_{QOOP-4}	0.92	0.69	0.63	0.89	0.85
3	25	I_n	I_{QOOP}	0.91	0.66	0.62	0.88	0.84
4	25	I_{QOOP-4}	I_n	0.91	0.69	0.61	0.86	0.84
5	25	I_{QOOP-4}	I_{QOOP-4}	0.93	0.79	0.70	0.90	0.88
6	25	I_{QOOP-4}	I_{QOOP}	0.93	0.76	0.66	0.90	0.87
7	25	I_{QOOP}	I_n	0.88	0.67	0.60	0.81	0.81
8	25	I_{QOOP}	I_{QOOP-4}	0.92	0.74	0.64	0.87	0.85
9	25	I_{QOOP}	I_{QOOP}	0.93	0.77	0.69	0.90	0.88
10	50	I_n	I_n	0.92	0.80	0.69	0.89	0.87
11	50	I_n	I_{QOOP-4}	0.92	0.71	0.62	0.89	0.85
12	50	I_n	I_{QOOP}	0.90	0.61	0.59	0.86	0.82
13	50	I_{QOOP-4}	I_n	0.91	0.72	0.62	0.87	0.85
14	50	I_{QOOP-4}	I_{QOOP-4}	0.92	0.78	0.67	0.89	0.87
15	50	I_{QOOP-4}	I_{QOOP}	0.92	0.76	0.65	0.89	0.86
16	50	I_{QOOP}	I_n	0.88	0.64	0.57	0.80	0.79
17	50	I_{QOOP}	I_{QOOP-4}	0.90	0.74	0.60	0.83	0.83
18	50	I_{QOOP}	I_{QOOP}	0.93	0.78	0.68	0.89	0.87
19	100	I_n	I_n	0.92	0.81	0.67	0.87	0.87
20	100	I_n	I_{QOOP-4}	0.91	0.79	0.62	0.87	0.86
21	100	I_n	I_{QOOP}	0.90	0.65	0.57	0.84	0.82

ISSN 1814-4225 (print)
ISSN 2663-2012 (online)

Continuation of the Table 5

Case	σ^2	Training Image	Classified Image	F1 class 3 (Urban)	F1 class 0 (Water)	F1 class 1 (Vegetation)	F1 class 2 (Bare soil)	F1 Total
22	100	I_{QOOP-4}	I_n	0.91	0.79	0.60	0.86	0.85
23	100	I_{QOOP-4}	I_{QOOP-4}	0.92	0.81	0.67	0.87	0.87
24	100	I_{QOOP-4}	I_{QOOP}	0.90	0.69	0.59	0.86	0.83
25	100	I_{QOOP}	I_n	0.88	0.72	0.56	0.80	0.80
26	100	I_{QOOP}	I_{QOOP-4}	0.89	0.73	0.57	0.81	0.82
27	100	I_{QOOP}	I_{QOOP}	0.92	0.79	0.66	0.87	0.86

When training the model on I_{QOOP-4} and evaluating on I_{QOOP-4} and I_{QOOP}, the weighted F1-score decreased as noise increased for both images (SS1 and SS2). During training on I_{QOOP}, similar trends were observed.

From the obtained results, it follows that it is best to use images with approximately the same noise level and compression factor for both model training and inference. A significant mismatch in noise levels between training and classification phases leads to a drop in performance, as the model learns features that are not present or are distorted in the test set. Moreover, using compressed images does not lead to a significant decrease in classification accuracy; at $\sigma^2 = 100$ and $Q = Q_{OOP}$, an accuracy of 0.96–0.97 for I_{QOPT-4} and I_{QOOP} observed, compared with about 0.95 for I_n. This implies that the loss of information during compression is compensated by the reduction of noise, which is particularly beneficial for the XGBoost algorithm.

It is worth noting that, in many cases, we obtained higher F1-scores than those reported in [18] for a simple neural network (NN) classifier based on multilayer perceptron (see Tables 6 and 7). XGBoost's decision-tree-based architecture appears more robust to outliers caused by noise than the MLP, which can overfit to specific noise patterns. For SS1, XGBoost outperformed the NN for all classes except Water and Vegetation, suggesting that the NN handled the classification of pixels in homogeneous regions better. This is likely because the NN can learn smoother decision boundaries for areas with low variance. Moreover, using the NN yielded higher F1-scores for all classes in the scenario where both training and testing were performed on $IQ_{OOP}-4$ at $\sigma^2 = 100$. For SS2, the XGBoost classifier produced a lower F1 for the Bare soil class, which in this image also corresponds to a relatively homogeneous area. The NN outperformed XGBoost in the compressed-and-noisy setting I_{QOOP-4}, $\sigma^2 = 100$. The noise-filtering effect induced by compression appears to have a stronger positive impact when using the NN, whereas our classifier is largely insensitive to it, exhibiting only small performance changes –either upward or downward, depending on the class.

It is also important to report the time spent on training and classification. Training used image fragments according to the provided masks. Each run of feature extraction, training, and classification produced slightly different timings: however, the values were close, and the differences can be attributed to background processes on the computation machine. Therefore, we report average values. Feature extraction for training took 0.18–0.20 seconds for SS1 and 0.1 seconds for SS2, which reflects the ratio of pixels in the masks. Feature extraction for the full image prior to classification took about 0.30 seconds for SS1 and 0.14 seconds for SS2. Model training required 4.0–4.5 seconds for SS1 and 3.5 seconds for SS2. Classification – i.e., generating the full image mask — took 1.2–1.5 seconds for both SS1 and SS2.

Examine the masks for the classified images. For SS1, the results are shown in Fig. 6.

Table 6

Comparative table of image classification results using a simple neural network (NN) and XGBoost (RGB+LBP) for SS1

	σ^2	Training Image	Classified Image	F1, Urban	F1, Water	F1, Vegetation	F1, Bare soil	F1, Total
XGBoost	25	I_n	I_n	0.89	0.99	0.94	0.87	0.96
NN		I_n	I_n	0.82	0.98	0.89	0.75	0.93
XGBoost		I_{QOOP-4}	I_{QOOP-4}	0.89	0.99	0.96	0.88	0.97
NN		I_{QOOP-4}	I_{QOOP-4}	0.85	1.00	0.96	0.84	0.97
XGBoost	50	I_n	I_n	0.88	0.99	0.93	0.86	0.96
NN		I_n	I_n	0.81	0.97	0.87	0.71	0.92
XGBoost		I_{QOOP-4}	I_{QOOP-4}	0.89	0.99	0.95	0.87	0.97
NN		I_{QOOP-4}	I_{QOOP-4}	0.88	1.00	0.96	0.86	0.97
XGBoost	100	I_n	I_n	0.88	0.98	0.92	0.86	0.95
NN		I_n	I_n	0.76	0.96	0.83	0.69	0.90
XGBoost		I_{QOOP-4}	I_{QOOP-4}	0.88	0.98	0.93	0.85	0.96
NN		I_{QOOP-4}	I_{QOOP-4}	0.89	1.00	0.96	0.89	0.97

Visually the largest number of errors is observed for the uncompressed image (Case 1). There are many misclassifications between the Water and Vegetation classes, specifically Vegetation pixels being labeled as Water. The masks for compressed images exhibit fewer obvious misclassifications, which is particularly noticeable for the Vegetation class. Thus, using compression at the OOP – which led to an increase in PSNR – also had a positive effect on overall classification accuracy. For S2, the results are presented in Fig. 7. Visually, the classification masks for compressed images look better, especially for homogeneous regions. The Bare soil class shows fewer false assignments to Vegetation.

Table 7

Comparative table of image classification results using a simple neural network (NN) and XGBoost (RGB+LBP) for SS2

	σ^2	Training Image	Classified Image	F1, Urban	F1, Water	F1, Vegetation	F1, Open Ground	F1, Total
XGBoost	25	I_n	I_n	0.93	0.79	0.70	0.91	0.88
NN		I_n	I_n	0.90	0.71	0.58	0.86	0.83
XGBoost		I_{QOOP-4}	I_{QOOP-4}	0.93	0.79	0.70	0.90	0.88
NN		I_{QOOP-4}	I_{QOOP-4}	0.92	0.69	0.71	0.93	0.87
XGBoost	50	I_n	I_n	0.92	0.80	0.69	0.89	0.87
NN		I_n	I_n	0.89	0.71	0.56	0.82	0.81
XGBoost		I_{QOOP-4}	I_{QOOP-4}	0.92	0.78	0.67	0.89	0.87
NN		I_{QOOP-4}	I_{QOOP-4}	0.92	0.72	0.73	0.93	0.88
XGBoost	100	I_n	I_n	0.92	0.81	0.67	0.87	0.87
NN		I_n	I_n	0.88	0.75	0.49	0.80	0.80
XGBoost		I_{QOOP-4}	I_{QOOP-4}	0.92	0.81	0.67	0.87	0.87
NN		I_{QOOP-4}	I_{QOOP-4}	0.93	0.72	0.72	0.92	0.88

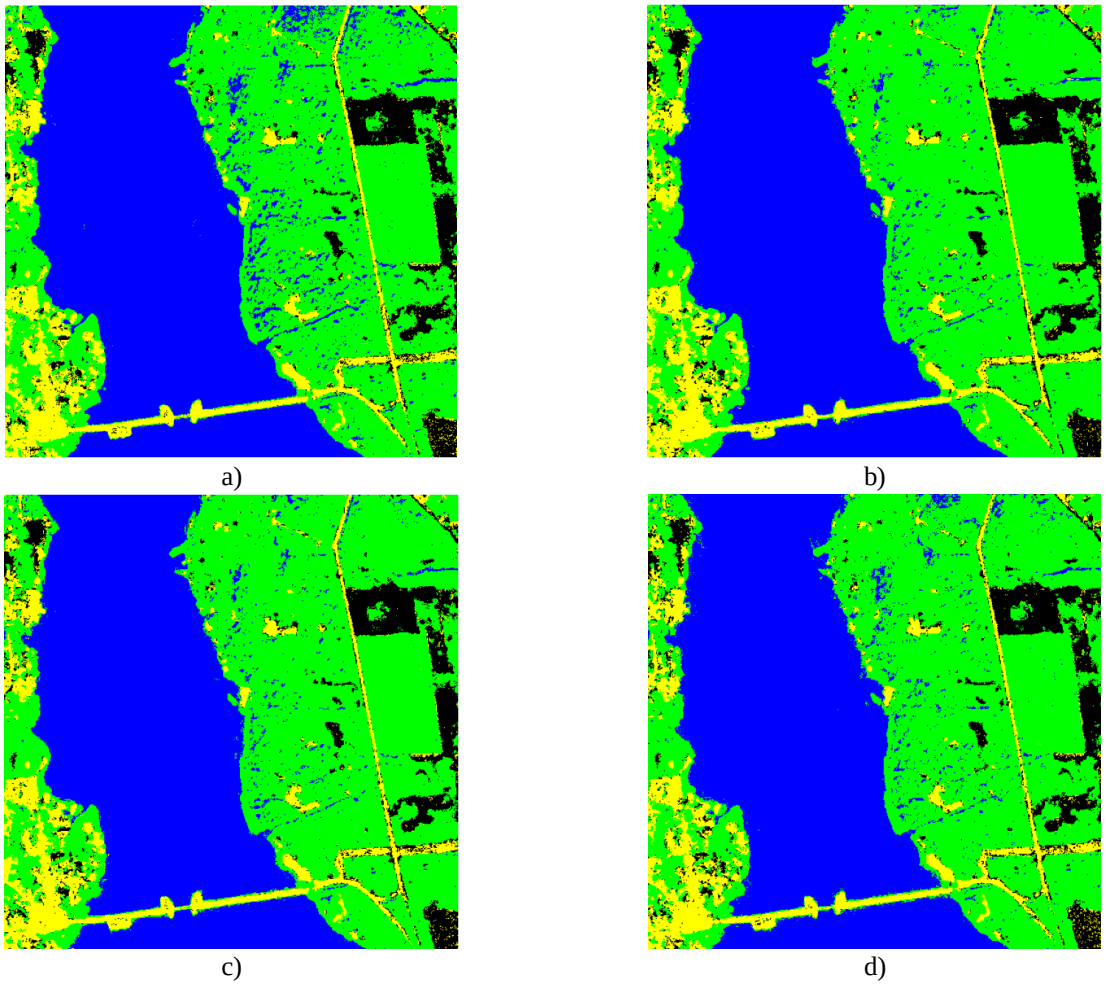

a) b) c) d)

Fig. 6. Classification results for image SS1, Case 1 (a) and Case 9 (b), Case 18 (c) and Case 27 (d)

ISSN 1814-4225 (print)
ISSN 2663-2012 (online)

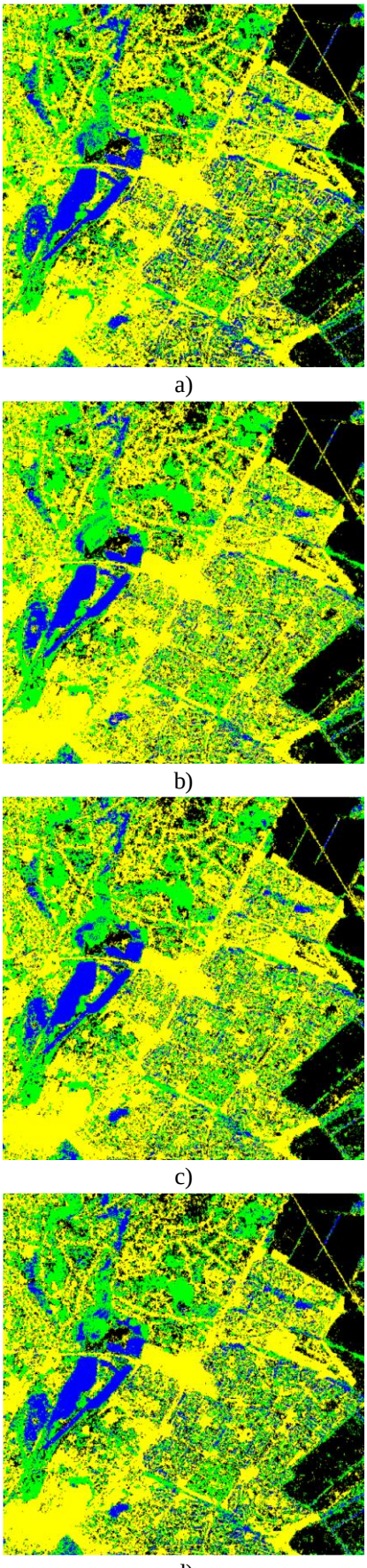

Fig. 7. Classification results for image SS2, Case 1 (a) and Case 9 (b), Case 18 (c) and Case 27 (d)

4. Conclusions

The study confirmed that the proposed classification method – combining LBP, channel features, and the XGBoost algorithm – is effective for satellite imagery even under challenging conditions, such as the presence of noise and compression-induced distortions due to lossy coding. Using LBP features proved beneficial, as they improved classification accuracy compared with relying on per-channel information alone. Moreover, LBP exhibited robustness to noise: evaluation metrics such as the F1 score were less sensitive to noise level than in the case of a neural network–based classifier. Importantly, LBP not only improves classification outcomes but is also computationally efficient due to its simple mathematical formulation.

Regarding the impact of compression, the model also proved fully competitive. Although strong compression somewhat affects the results, overall accuracy remains at an acceptable level even at relatively high Q values for BPG. A specific issue does arise on homogeneous surfaces such as water. Despite LBP's ability to capture texture characteristics, compressed images exhibited artifacts stemming from the interaction between BPG compression and LBP. This was especially evident in situations where texture homogeneity makes the model more sensitive to compression-induced distortions. Thus, there is potential to refine the LBP configuration to reduce artifacts that appear under compression on homogeneous surfaces.

A comparison with a simple NN has showed that the XGBoost-based classifier generally exhibits greater stability and accuracy, especially for texture-rich classes such as Urban areas, even under challenging noise and compression conditions. At the same time, the NN demonstrated an advantage on homogeneous and relatively homogeneous regions – particularly for Water (SS1) and Bare soil (SS2) – where its accuracy was higher in some cases.

Adapting LBP parameters and refining approaches for processing surfaces with different degrees of homogeneity may become an important direction for future work. Promising avenues include incorporating compression parameters at the model design stage and investigating how to adapt the classifier to diverse noise types and image texture regimes.

Contributions of authors: conceptualization, methodology – **Sergii Kryvenko;** formulation of tasks, analysis – **Sergii Kryvenko, Maksym Rybnytksyi;** original data preparation **Volodymyr Rebrov;** development of model, software - **Maksym Rybnytksyi**, verification – **Volodymyr Lukin, Maksym Rybnytskyi;** analysis of results, visualization – **Maksym Rybnytskyi;**

writing – original draft preparation – **Maksym Rybnytskyi**, writing – review and editing **– Volodymyr Lukin.**

Conflict of Interest

The authors declare that they have no conflict of interest in relation to this research, whether financial, personal, author ship or otherwise, that could affect the research and its results presented in this paper.

Financing

The research has been funded by National Research Foundation of Ukraine (https://nrfu.org.ua/en/, accessed on 1 July 2025) within Project No. 2023. 04/0039 “Geospatial monitoring system for the war impact on the agriculture of Ukraine based on satellite data” (2024–2025).

Data Availability

Data will be made available upon reasonable request.

Use of Artificial Intelligence

The authors have used artificial intelligence technologies within acceptable limits to provide their own verified data, as described in the research methodology section.

Acknowledgments

All the authors have read and agreed to the published version of this manuscript.

References

1. Li, Z., Chen, B., Wu, S., Su, M., Chen, J. M. and Xu, B. Deep learning for urban land use category classification: A review and experimental assessment, *Remote Sensing of Environment*, 2024, vol. 311. DOI: 10.1016/j.rse.2024.114290.

2. Kussul N.M., Shelestov, A. Y., Lavreniuk, A. M., Yailymov, B. Ya., Yailymova, H. O., Kolotii, A. V., Drozd, S. Yu., Savin, V. V., Mikava, P. V., Kyrylenko, I. A., Yavorskyi, O. A., Okhrimenko, A. O., Parkhomchuk, O. M., Khar, D. F. and Volkova, E. A. *Metody komp'juternogho zoru i ghlybynnykh nejronnykh merezh dlja ekologho-ekonomichnogho analizu*. Kyyiv: Naukova dumka, 2024, 474 p.

3. De Jong, S. and Meer, F. *Remote Sensing Image Analysis: Including The Spatial Domain*. Springer Dordrecht, 2007, 359 p. DOI: 10.1007/978-1-4020-2560-0.

4. West, H., Quinn, N. and Horswell, M. Remote sensing for drought monitoring & impact assessment: Progress, past challenges and future opportunities, *Remote Sensing of Environment*, 2019, vol. 232. DOI: 10.1016/j.rse.2019.111291.

5. Ma, X. High-resolution image compression algorithms in remote sensing imaging, *Displays*, 2023, vol. 79. DOI: 10.1016/j.displa.2023.102462.

6. Abramova, V., Lukin, V., Abramov, S., Abramov, K. and Bataeva, E. Analysis of Statistical and Spatial Spectral Characteristics of Distortions in Lossy Image Compression, in *2022 IEEE 2nd Ukrainian Microwave Week (UkrMW)*, 2022, pp 644–649. DOI: 10.1109/UkrMW58013.2022.10036949.

7. Fırat, H., Asker, M. E., Bayindir, M. İ. and Hanbay, D. Spatial-spectral classification of hyperspectral remote sensing images using 3D CNN based LeNet-5 architecture, *Infrared Physics & Technology*, 2022, vol. 127. DOI: 10.1016/j.infrared.2022.104470.

8. Proskura, G., Vasilyeva, I. and Lukin, V. Analysis of Improvement of Noisy Multichannel Image Controlled Pixel-by-Pixel Classification by Post-Classification Processing, in *2020 IEEE 15th International Conference on Advanced Trends in Radioelectronics, Telecommunications and Computer Engineering (TCSET)*, 2020, pp 1–6. DOI: 10.1109/TCSET49122.2020.235488.

9. Cheng, G., Han, J. and Lu, X. Remote Sensing Image Scene Classification: Benchmark and State of the Art, *Proceedings of the IEEE*, 2017, vol. 105, no. 10, pp 1865–1883. DOI: 10.1109/JPROC.2017.2675998.

10. Bioucas-Dias, J. M., Plaza, A., Camps-Valls, G., Scheunders, P., Nasrabadi, N. and Chanussot, J. Hyperspectral Remote Sensing Data Analysis and Future Challenges, *IEEE Geoscience and Remote Sensing Magazine*, 2013, vol. 1, no. 2, pp 6–36. DOI: 10.1109/MGRS.2013.2244672.

11. S, P. Image Classification Using Machine Learning Approaches, *INTERNATIONAL JOURNAL OF CREATIVE RESEARCH THOUGHTS*, 2023, vol. 11, pp B816–B819.

12. Kovalenko, B., Lukin, V., Kryvenko, S., Naumenko, V. and Vozel, B. Prediction of parameters in optimal operation point for BPG-based lossy compression of noisy images, *Ukrainian journal of remote sensing*, 2022, vol. 9, no. 2, pp 4–12.

13. Radosavljević, M., Brkljač, B., Lugonja, P., Crnojević, V., Trpovski, Ž., Xiong, Z. and Vukobratović, D. Lossy Compression of Multispectral Satellite Images with Application to Crop Thematic Mapping: A HEVC Comparative Study, *Remote Sensing*, 2020, vol. 12, no. 10. DOI: 10.3390/rs12101590.

14. Jiao, W., Hao, X. and Qin, C. The Image Classification Method with CNN-XGBoost Model Based on Adaptive Particle Swarm Optimization, *Information*, 2021, vol. 12, no. 4. DOI: 10.3390/info12040156.

15. Boonprong, S., Cao, C., Chen, W., Ni, X., Xu, M. and Acharya, B. K. The Classification of Noise-Afflicted Remotely Sensed Data Using Three Machine-Learning Techniques: Effect of Different Levels and Types of Noise on Accuracy, *ISPRS International Journal of Geo-Information*, 2018, vol. 7, no. 7. DOI: 10.3390/ijgi7070274.

16. Ahmed, T. S., Sayed, A. N., Youssef, A., Shaker, G. and Elbahnasawy, M. Assessing Noise Effects on UAV Classification Accuracy With Deep Learning and FPGA Real-Time Processing: A Study Utilizing Radar Digital Twins, *IEEE Sensors Journal*, 2025, vol. 25, no. 12, pp 22850–22862. DOI: 10.1109/JSEN.2025.

ISSN 1814-4225 (print)
ISSN 2663-2012 (online)

3566651.

17. Proskura, G., Vasilyeva, I., Li, F. and Lukin, V. Classification of Compressed Multichannel Images and Its Improvement, in *2020 30th International Conference Radioelektronika (RADIOELEKTRONIKA)*, 2020, pp 1–6. DOI: 10.1109/RADIOELEKTRONIKA49387.2020.9092371.

18. Rebrov, V., Proskura, G. and Lukin, V. Classification of Compressed Noisy Three-Channel Noisy Images: Comparison of Several Approaches, *Integrated Computer Technologies in Mechanical Engineering - 2024. ICTM 2024* [Preprint], 2025.

19. Vawda, M. I., Lottering, R., Mutanga, O., Peerbhay, K. and Sibanda, M. Comparing the Utility of Artificial Neural Networks (ANN) and Convolutional Neural Networks (CNN) on Sentinel-2 MSI to Estimate Dry Season Aboveground Grass Biomass, *Sustainability*, 2024, vol. 16, no. 3. DOI: 10.3390/su16031051.

20. Chugh, R., Bhatia, V., Khanna, K. and Bhatia, V. A Comparative Analysis of Classifiers for Image Classification, in, 2020, pp 248–253. DOI: 10.1109/Confluence47617.2020.9058042.

21. Chakraborty, D. and Elzarka, H. Advanced machine learning techniques for building performance simulation: a comparative analysis, *Journal of Building Performance Simulation*, 2018, vol. 12, pp 1–15. DOI: 10.1080/19401493.2018.1498538.

22. Song, Y., Zhang, J., Liu, Z., Xu, Y., Quan, S., Sun, L., Bi, J. and Wang, X. Deep learning for hyperspectral image classification: A comprehensive review and future predictions, *Information Fusion*, 2025, vol. 123. DOI: 10.1016/j.inffus.2025.103285.

23. Ahmad, M., Shabbir, S., Roy, S. K., Hong, D., Wu, X., Yao, J., Khan, A. M., Mazzara, M., Distefano, S. and Chanussot, J. Hyperspectral Image Classification—Traditional to Deep Models: A Survey for Future Prospects, *IEEE Journal of Selected Topics in Applied Earth Observations and Remote Sensing*, 2022, vol. 15, pp 968–999. DOI: 10.1109/JSTARS.2021.3133021.

24. Pietikäinen, M., Hadid, A., Zhao, G. and Ahonen, T. *Computer Vision Using Local Binary Patterns*, 2011. DOI: 10.1007/978-0-85729-748-8.

25. *XGBoost Documentation — xgboost 3.0.2 documentation*. Available at: https://xgboost.readthedocs.io/en/stable/ (accessed 05.06.2025).

26. *BPG Image format*. Available at: https://bellard.org/bpg/ (accessed 13.07.2025).

27. Proskura, G., Naumenko, V. and Lukin, V. Classification of BPG-Based Lossy Compressed Noisy Images, *Ukrainian journal of remote sensing*, 2024, vol. 11, no. 3, pp 13–25. DOI: 10.36023/ujrs.2024.11.3.266.

28. *Local Binary Pattern for texture classification — skimage 0.25.2 documentation*. Available at: https://scikit-image.org/docs/0.25.x/auto_examples/features_detection/plot_local_binary_pattern.html (accessed 08.08.2025).

29. Ojala, T., Pietikainen, M. and Maenpaa, T. Multiresolution gray-scale and rotation invariant texture classification with local binary patterns, *IEEE Transactions on Pattern Analysis and Machine Intelligence*, 2002, vol. 24, no. 7, pp 971–987. DOI: 10.1109/TPAMI.2002.1017623.

30. Punia, R. How to Measure the Performance of Your Machine Learning Models: Precision, Recall, Accuracy, and F1 score, *Medium*. Available at: https://rspunia.medium.com/how-to-measure-the-performance-of-your-machine-learning-models-precision-recall-accuracy-and-f1-855702df048b (accessed 10.01.2025).

Received 28.08.2025, Received in revised form 15.09.2025
Accepted date 03.11.2026, Published date 08.12.2025

КОМБІНОВАНИЙ ПІДХІД ДО ПІКСЕЛЬНОЇ КЛАСИФІКАЦІЇ СУПУТНИКОВИХ ЗОБРАЖЕНЬ НА ОСНОВІ LBP, ПСЕВДОКОЛЬОРОВИХ ОСОБЛИВОСТЕЙ ТА XGBOOST

М. А. Рибницький, С. С. Кривенко, В. В. Лукін, В. С. Ребров

Предметом статті є попіксельна класифікація супутникових зображень Sentinel-2, представлених як триканальні дані, приведені до простору RGB для зручної візуалізації, з особливою увагою до викликів, зумовлених сенсорним шумом і артефактами стиснення з втратами, типовими для супутникових даних. **Мета** полягає у розробленні та валідації підходу до класифікації, який зберігає високу точність за умов значного шуму та стиснення, поєднуючи текстурні дескриптори Local Binary Patterns (LBP) із псевдокольоровими ознаками та використовуючи ефективний ансамблевий класифікатор. **Завдання**, які необхідно вирішити: спроєктувати компактне подання ознак, що інтегрує текстурну інформацію на основі LBP із псевдокольором; навчити та налаштувати класифікатор XGBoost на цих ознаках і порівняти його роботу з базовими підходами, які використовують лише псевдокольорову інформацію, а також із простими моделями нейронних мереж; оцінити стійкість до шуму та артефактів стиснення в діапазоні рівнів компресії. Використані **методи** включають вилучення дескрипторів LBP для фіксації локальних текстурних шаблонів, формування псевдокольорових ознак із каналів Sentinel-2, відображених у RGB, та поєднання цих дескрипторів у спільні вектори ознак. Для побудови моделі класифікації застосовано алгоритм XGBoost. Ефективність моделі оцінюється за метрикою F1 як основною, за різних умов шуму та стиснення. Додатково використовується візуальний аналіз отриманих класифікаційних мап для підтвердження кількісних результатів і аналізу просторової узгодженості та профілю

помилок. **Висновки.** Наукова новизна отриманих результатів полягає в наступному: вперше для задачі попіксельної класифікації Sentinel-2 системно досліджено й обґрунтовано використання LBP у поєднанні з XGBoost у сценаріях стиснення з втратами BPG при роботі в оптимальній робочій точці (OPT) або поблизу неї; експериментально встановлено суттєвий приріст у точності екласифікації для неоднорідних класів (урбанізовані території, рослинність, відкритий ґрунт) і обмежений — для однорідних (вода), а також зафіксовано артефакти взаємодії BPG+LBP на однорідних поверхнях і окреслено напрям адаптації параметрів LBP для їхнього зменшення; показано обчислювальну придатність підходу (час виділення ознак, навчання та класифікації) для операційних конвеєрів; проведено порівняння з простою нейронною мережею і продемонстровано вищу стабільність запропонованого підходу на текстурно насичених класах за умов шуму та стиснення, що задає межі застосовності альтернативних методів. Дослідження також показує, що врахування ефектів стиснення важливе для операційних конвеєрів обробки: стиснення зображень до оптимальної робочої точки може зменшити обсяг даних і, у деяких випадках, трохи поліпшити точність класифікації завдяки послабленню шуму.

Ключові слова: класифікація; супутникові зображення; Local Binary Patterns; XGBoost; шум; стиснення.

Рибницький Максим Анатолійович – асп. каф. інформаційно-комунікаційних технологій ім. О. О. Зеленського, Національний аерокосмічний університет «Харківський авіаційний інститут», Харків, Україна.

Кривенко Сергій Станіславович – канд. техн. наук, старш. наук. співроб. каф. інформаційно-комунікаційних технологій ім. О. О. Зеленського, Національний аерокосмічний університет «Харківський авіаційний інститут», Харків, Україна.

Лукін Володимир Васильович – д-р техн. наук, проф., зав. каф. інформаційно-комунікаційних технологій ім. О. О. Зеленського, Національний аерокосмічний університет «Харківський авіаційний інститут», Харків, Україна.

Ребров Володимир Сергійович – ас. каф. інформаційно-комунікаційних технологій ім. О. О. Зеленського, Національний аерокосмічний університет «Харківський авіаційний інститут», Харків, Україна.

Maksym Rybnytskyi – PhD Student of the Department of Information-Communication Technologies named after O. O. Zelensky, National Aerospace University "Kharkiv Aviation Institute", Kharkiv, Ukraine,
e-mail: m.a.rybnytskyi@khai.edu, ORCID: 0009-0000-1299-1604.

Sergii Kryvenko – PhD of Technical Science, Senior Research Scientist at the Department of Information-Communication Technologies named after O. O. Zelensky, National Aerospace University "Kharkiv Aviation Institute", Kharkiv, Ukraine,
e-mail: v.naumenko@khai.edu, ORCID: 0000-0002-5291-6032.

Volodymyr Lukin – Doctor of Technical Science, Professor, Head of the Department of Information-Communication Technologies named after O. O. Zelensky, National Aerospace University “Kharkiv Aviation Institute”, Kharkiv, Ukraine,
e-mail: v.lukin@khai.edu, ORCID: 0000-0002-1443-9685.

Volodymyr Rebrov – PhD Student of the Department of Information-Communication Technologies named after O. O. Zelensky, National Aerospace University "Kharkiv Aviation Institute", Kharkiv, Ukraine,
e-mail: mr.vladimirrebrov@gmail.com, ORCID: 0000-0002-6442-3155.